nature materials

ARTICLES

PUBLISHED ONLINE: 20 OCTOBER 2013 | DOI: 10.1038/NMAT3778

Highly sensitive nanoscale spin-torque diode

S. Miwa[1†], S. Ishibashi[1,2†], H. Tomita[1], T. Nozaki[1,2], E. Tamura[1], K. Ando[1], N. Mizuochi[1], T. Saruya[2‡], H. Kubota[2], K. Yakushiji[2], T. Taniguchi[2], H. Imamura[2], A. Fukushima[2], S. Yuasa[2] and Y. Suzuki[1,2*]

Highly sensitive microwave devices that are operational at room temperature are important for high-speed multiplex telecommunications. Quantum devices such as superconducting bolometers possess high performance but work only at low temperature. On the other hand, semiconductor devices, although enabling high-speed operation at room temperature, have poor signal-to-noise ratios. In this regard, the demonstration of a diode based on spin-torque-induced ferromagnetic resonance between nanomagnets represented a promising development, even though the rectification output was too small for applications (1.4 mV mW^{-1}). Here we show that by applying d.c. bias currents to nanomagnets while precisely controlling their magnetization-potential profiles, a much greater radiofrequency detection sensitivity of 12,000 mV mW^{-1} is achievable at room temperature, exceeding that of semiconductor diode detectors (3,800 mV mW^{-1}). Theoretical analysis reveals essential roles for nonlinear ferromagnetic resonance, which enhances the signal-to-noise ratio even at room temperature as the size of the magnets decreases.

New and desirable characteristics in magnetic nanomaterials, such as large magnetoresistance[1–7], spin-transfer-induced magnetization switching[8–13], and excitation of spin precession[14–16], have been observed in the emerging field of spintronics, in which two attributes of the electron, namely charge and spin, are simultaneously manipulated. These characteristics have been exploited in the development of magnetic pick-up sensors in magnetic hard disk drives, resulting in a massive increase in the storage density of these drives. This has led to the expectation that spintronics would one day emerge as a viable post-CMOS (complementary metal–oxide–semiconductor) technology. In this research direction, there are several interesting advancements[17–19]. However, spintronic devices have yet to exceed or meet the basic functionalities of traditional semiconductor devices, that is, diode or transistor operations. In 2005, the rectification of radiofrequency (RF) signals using magnetic tunnel junctions (MTJs) was demonstrated by using a combination of a large magnetoresistance and ferromagnetic resonance (FMR) induced by spin-transfer torque, which resulted in a phenomenon referred to as the spin-torque diode effect[20]. This enabled the quantitative measurement of spin torques and helped clarify their underlying physics[21–25]. However, the RF detection sensitivity in the first report[20] (1.4 mV mW^{-1}, defined as the detection voltage, V_{detect}, divided by the RF input power, P_{RF}) was more than three orders lower than that of semiconductor Schottky diode detectors (3,800 mV mW^{-1}). Many efforts such as the control of magnetic field direction[26–28], and the use of stochastic resonance[29] and voltage torque[30] have significantly enhanced the sensitivity. Nevertheless, the sensitivity of MTJs remains far lower than that of semiconductor diode detectors (see Supplementary Information 1).

Here we show that the application of a d.c. bias current to a MTJ along with the precise control of their magnetization-potential profiles affords a high RF detection sensitivity of 12,000 mV mW^{-1} at room temperature, which exceeds that of semiconductor Schottky diode detectors. Analysis based on a macro-spin model revealed that the increase is caused by nonlinear FMR (ref. 24) explained as the rotation of the precession axis that depends on the RF-signal input power (Fig. 1a). We found that this rotation, a nonlinear effect, results in a large change in resistance and affords higher sensitivity. In addition, we found that the nonlinear effect enhances signals more than noise as the size of the magnets decreases. Therefore, the signal-to-noise ratio may reach the thermodynamic limit in ~10-nm-scale junctions. This demonstrates that a spintronics device may overcome the limitations of semiconductor devices and eventually reach thermodynamic limits.

In semiconductor diodes, the band bending of junction interfaces, caused by a space charge, induces a nonlinear effect called rectification. In RF detectors based on MTJs, this nonlinear effect is induced by the magnetization dynamics due to current injection, FMR induced by spin-transfer torque as mentioned earlier, and a subsequent resistance change[20]. In this study, we used MTJ devices with MgO tunnel barriers, which are known to have a large magnetoresistance[4–7]. To obtain a higher sensitivity than that of semiconductors, a large response in magnetization precessional motion has to be excited under a small spin torque. To this end, the FMR frequency in the free-layer magnetization was synchronized with that of the detected RF input so as to efficiently excite magnetization precession. In addition, small in-plane and out-of-plane (perpendicular) magnetic anisotropy fields were prepared to obtain larger precession orbitals; the preparation of these fields involved designing a circle-shaped sample, 120 nm in diameter, and employing a FeB free layer with a MgO cap with perpendicular anisotropy[31]. The perpendicular anisotropy field almost compensated for the out-of-plane demagnetization field and made the total anisotropy of the films small.

[1]Graduate School of Engineering Science, Osaka University, Toyonaka, Osaka 560-8531, Japan, [2]National Institute of Advanced Industrial Science and Technology (AIST), Spintronics Research Center, Tsukuba, Ibaraki 305-8568, Japan. †These authors contributed equally to this work. ‡Present address: Process Development Center, Canon ANELVA Corporation, Kawasaki, Kanagawa 215-8550, Japan. *e-mail: suzuki-y@mp.es.osaka-u.ac.jp

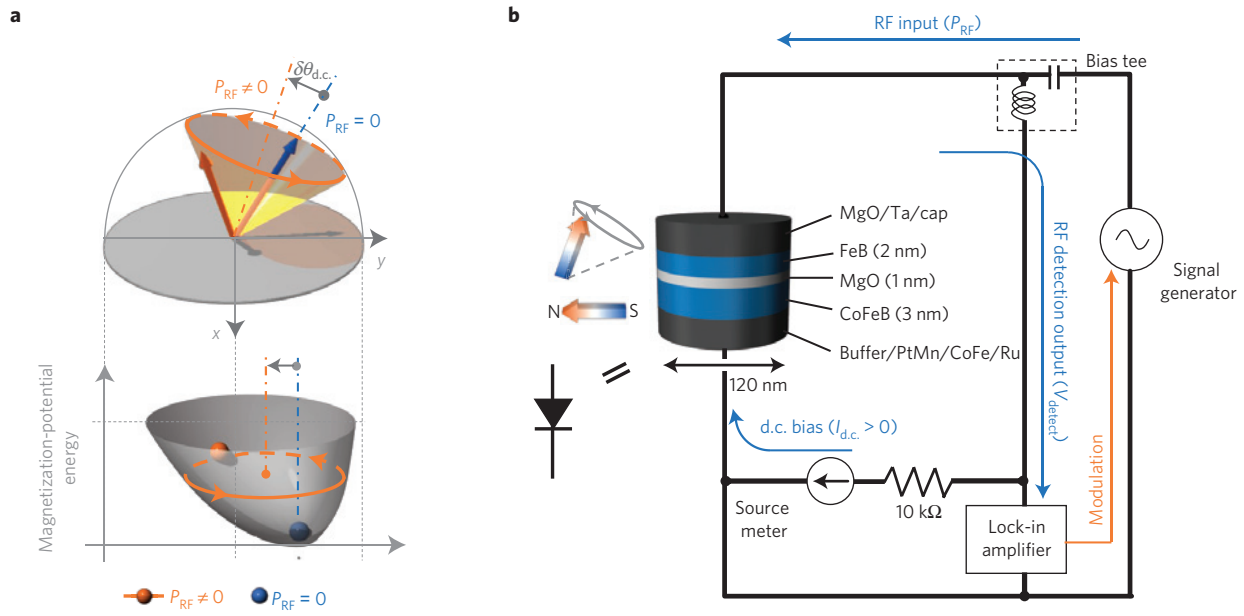

Figure 1 | Nonlinear effect in nanomagnets and the spin-torque diode device. a, Schematic image of a nonlinear effect in nanomagnets. Under FMR with an asymmetrical potential, the orbital centre of the free-layer magnetization ($P_{RF} \neq 0$, orange) rotates away from the initial state ($P_{RF} = 0$, blue), causing a change in the average resistance; the application of a d.c. bias converts the average resistance change into a large RF detection voltage. **b**, Spin-torque diode device and measurement set-up. The device is based on a MTJ with a MgO tunnel barrier and FeB magnetic free layer. The RF detection output of the MTJ is measured by a low-frequency (10 kHz) modulation method, using a lock-in amplifier.

Figure 1b illustrates the structure of the MTJ used in our experiments. In MTJs, the junction resistance depends on the relative angle (θ_{12}) between the magnetizations in the free and pinned layers

$$R^{-1}(\theta_{12}) = \frac{R_P^{-1} + R_{AP}^{-1}}{2} + \frac{R_P^{-1} - R_{AP}^{-1}}{2}\cos\theta_{12} \quad (1)$$

where the resistances in the parallel (R_P) and anti-parallel (R_{AP}) configurations are 210 Ω and 390 Ω, respectively. When an RF current was applied, a precessional motion was excited only in the free layer, because the magnetization in the pinned layer was fixed by an exchange bias layer (Methods). A dynamic resistance change due to the precessional motion produced a d.c. voltage. The measurement circuit for RF detection is also shown in Fig. 1b. An RF current input and a d.c. bias were applied to the device using a signal generator (E8257D, Agilent Technologies) and a source meter (2400, Keithley), respectively. To separate the RF detection voltage that originated in the MTJs from the d.c. bias, the RF input was modulated at a low frequency (10 kHz) and a signal synchronized with the modulation was measured with a lock-in amplifier (SR830, Standard Research Systems). Magnetic field was applied using a probe system with a three-dimensional vector electromagnet (Toei Scientific Industrial).

The junction resistance was measured as a function of the applied magnetic field (Fig. 2a) to understand the magnetization process. The field was applied in a direction that tilts 10° from the z axis towards the anti-parallel direction (y axis) with respect to the pinned-layer magnetization. Here, the z axis and the y axis were perpendicular and parallel to the film plane, respectively (Fig. 2a, inset). From equation (1), the relative angle between the free and pinned layers was calculated and is shown on the right-hand axis in Fig. 2a. In Fig. 2a inset, the magnetization process of the free-layer magnetization is schematically illustrated. Without the magnetic field, the magnetization in the free layer was nearly aligned with the x axis because there exists the small structural in-plane anisotropy although the designed junction shape was a circle. By the application of a small magnetic field, the magnetization turned in-plane towards the y axis. As the field became larger, the out-of-plane component appeared. The hysteresis observed in Fig. 2a probably results from the motion of the pinned-layer magnetization. Figure 2b shows the (linear) FMR frequency of the precession in the free-layer magnetization under perpendicular (0°) and 10° tilted applied magnetic fields. As the FMR frequency corresponds to the second derivative of the magnetization-potential energy with respect to the polar and/or azimuth angles, the anisotropy fields that describe the model of magnetic anisotropy energy in the free layer were obtained from a fitting[32]. For the fit, the stray field from the pinned-layer magnetization was not considered. The grey solid line represents the resonant frequencies calculated from the model. From the fit, the perpendicular anisotropy (hard axis is z) and the in-plane anisotropy (hard axis is y) fields were estimated to be 0.9 kOe and 0.035 kOe, respectively. Both of these values are small compared with those in previous studies, and a condition in which the free-layer magnetization easily oscillates was obtained.

Then, RF detection measurements were conducted under the magnetic field condition of $H = 1.1$ kOe and 10° tilted from the film normal. To obtain stable precession orbitals, a field slightly larger than the perpendicular anisotropy field (0.9 kOe) was applied. A magnetic field whose direction was tilted from the normal to the film plane was employed to break the symmetry of the potential. The magnetization potential in the free layer is shown in Fig. 1a. The aforementioned factors allowed us to excite the nonlinear FMR, a phenomenon that is described in Fig. 1a and explained in detail later. All measurements were conducted at room temperature (for the magnetic field condition, see also Supplementary Information 2). Owing to the magnetic field conditions, which enable a stable magnetization precession, we could obtain nearly the same response, including small in-plane anisotropy, from most of samples in the same batch.

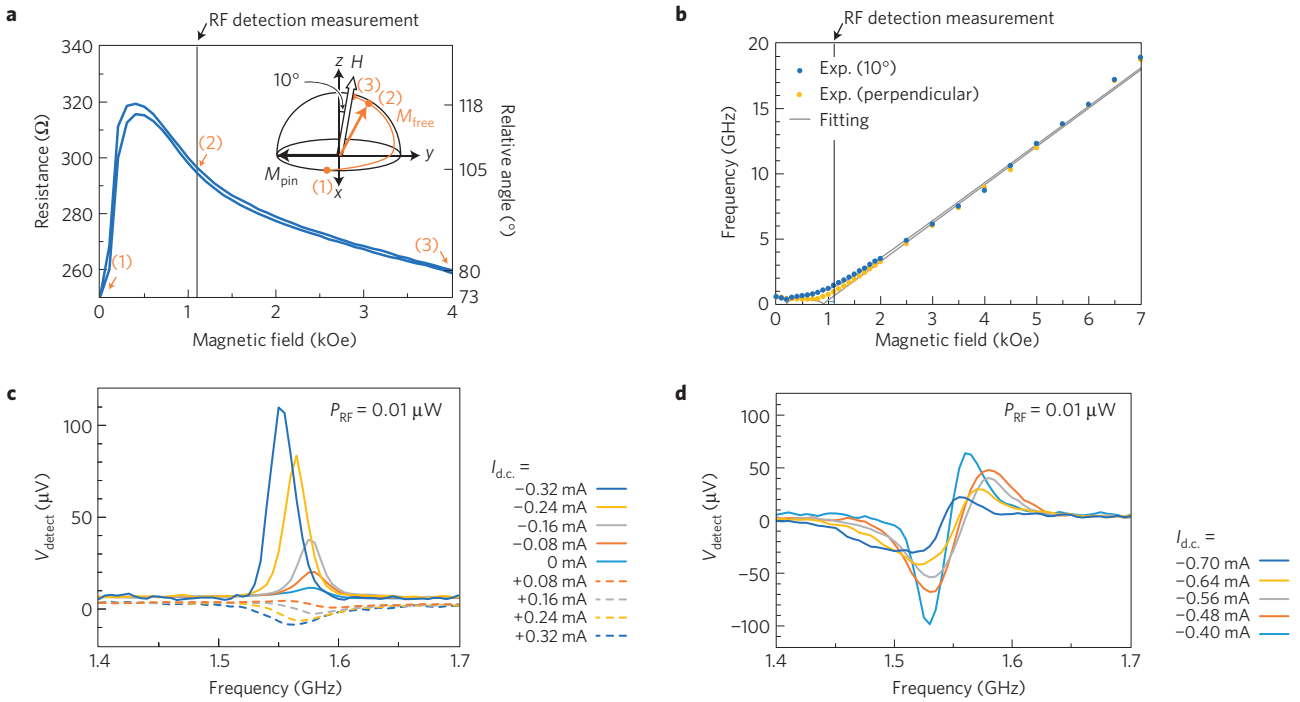

Figure 2 | Basic device characteristics. a, The device resistance as a function of the applied magnetic field. The right axis represents the relative angle between the magnetization directions of the free (FeB) and pinned (CoFeB) layers, which is calculated from equation (1). The orange curve in the inset shows the schematic path of the free-layer magnetization direction ($\mathbf{M}_{free}$). The black ($\mathbf{M}_{pin}$) and white ($\mathbf{H}$) arrows represent the direction of the pinned-layer magnetization and the applied magnetic field, respectively. RF detection measurements were conducted under the magnetic field condition of $H = 1.1$ kOe, where a large relative angle between $\mathbf{M}_{free}$ and $\mathbf{M}_{pin}$ is realized. **b**, The ferromagnetic resonant frequency of the free layer as a function of the applied magnetic field. From the fits (grey solid curves), the perpendicular anisotropy (hard axis is z) and the in-plane anisotropy (hard axis is y) fields were estimated to be 0.9 and 0.035 kOe, respectively. Both of these values are small compared with those in previous studies, and a condition in which the free-layer magnetization easily oscillates under a shallow magnetization-potential was obtained. From the analysis, magnetization potential in the free layer is determined (see Fig. 1a). **c**,**d**, The RF detection voltage (V_{detect}) as a function of the RF input frequency under various d.c. bias currents ($I_{d.c.}$) The RF input power (P_{RF}) is 0.01 μW (4.8 μA). A large output voltage was obtained at the resonant frequency, and d.c. bias was found to enhance the detection voltage.

Figure 2c shows the RF detection voltage (V_{detect}) as a function of the applied RF frequency. The input RF power (P_{RF}) was 0.01 μW (4.8 μA). A large output voltage was obtained at the FMR frequency. The very small spectrum indicated by the solid curve in light blue was measured under zero d.c. bias; it corresponds to the known spin-torque diode spectrum, which originates from the FMR induced by spin-transfer torque[20]. The RF detection mechanism under zero d.c. bias is explained as the homodyne detection of the applied RF current because of the oscillation of resistance at the same frequency. In the first report[20], the RF detection output is approximately 45 μV under a zero d.c. bias when $P_{RF} = 32$ μW is applied, resulting in a detection sensitivity of 1.4 mV mW^{-1}. In our study, we obtained a high sensitivity of 630 mV mW^{-1} under a zero d.c. bias, which is 450 times greater than the first report.

In this study, both negative and positive d.c. biases were found to enhance the detection voltage, as shown in Fig. 2c. The enhancement under negative d.c. bias was greater; under negative d.c. bias, the detection voltage was up to 20 times that under zero d.c. bias voltage. The results are consistent with a theoretical expectation. Under a negative d.c. bias, the spin-transfer torque should decrease the damping of the precession in the free-layer magnetization. However, on the application of the large negative d.c. bias current (Fig. 2d), the spectrum changed to a dispersion shape, and the detection voltage decreased. This result may relate to a destabilization of the anti-parallel state because of large anti-damping.

Figure 3a shows the RF detection voltage (taken as the peak value in Fig. 2c,d) as a function of the d.c. bias current. Figure 3b shows the RF detection sensitivity (V_{detect}/P_{RF}) as a function of the RF input power. Under small input power, the sensitivity is constant, and the system shows quadratic detection properties (power detection). The maximum sensitivity to the input power in the transmission line is 12,000 mV mW^{-1}, which is three times that of semiconductor Schottky diode detectors (3,800 mV mW^{-1}). The results indicate that the spin-torque diode effect in MTJs is suitable for the highly sensitive detection of small RF signals.

To estimate the critical current (I_c) at which the anti-parallel configuration of the magnetization is destabilized by the spin-transfer torque, the spectral linewidths of the FMR spectra were plotted as a function of the d.c. bias current ($I_{d.c.}$), as shown in Fig. 3c. As the linewidth is proportional to the effective damping of the precession, the reduction of the linewidth by the negative d.c. bias indicates a decrease in the damping[33,34]. When the damping reaches zero, magnetization switching or auto-oscillation occurs. Therefore, the critical current is estimated to be $I_c = -0.42$ mA from the extrapolation of the fit line in Fig. 3c. Around I_c, the linewidth exhibits a local maxima, which has already been predicted[34]. From Fig. 3a, a maximum detection voltage is obtained near $I_{d.c.} = I_c$. Thus, we can expect a strong relation between the enhancement of the RF detection voltage and the reduction in damping due to the spin-transfer torque.

To quantitatively characterize the enhancement of the RF detection voltage, we obtained the analytical solutions of the magnetization motion induced by an RF current under the assumption that in the macro-spin dynamics, all spins in a magnetic cell align in parallel and show coherent motion. Such macro-spin

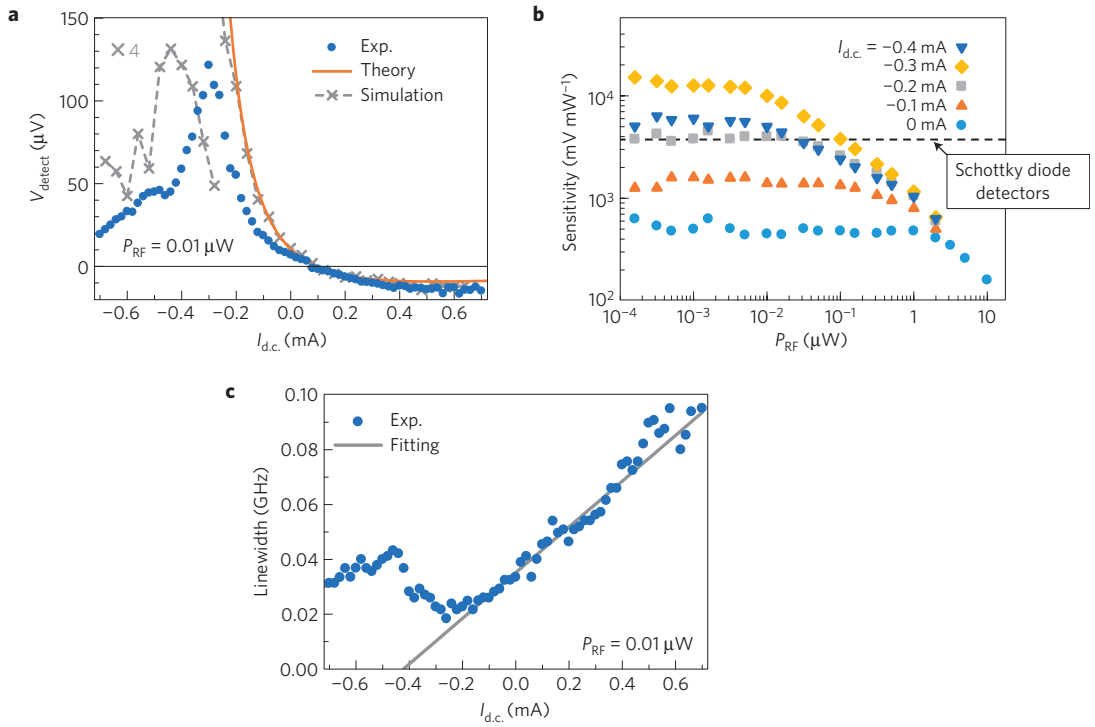

Figure 3 | d.c. bias and RF input power dependence. a, The RF detection voltage (V_{detect}) as a function of the d.c. bias ($I_{d.c.}$). The solid orange curve and the grey dotted curve represent the theoretical values obtained from equation (4) and macro-spin simulation, respectively. The enhancement of the detection voltage under d.c. bias was well explained by a nonlinear effect which is described in Fig. 1a. **b**, The RF detection sensitivity (V_{detect}/P_{RF}) as a function of the RF input power (P_{RF}). The maximum sensitivity is 12,000 mV mW^{-1}, greater than that of the semiconductor Schottky diode detectors (3,800 mV mW^{-1}). **c**, Spectral linewidths of the FMR in the free-layer magnetizations as a function of the d.c. bias current ($I_{d.c.}$). By extrapolating the fitting line (grey solid line), the critical current for magnetization stability in the free layer is estimated to be $I_c = -0.42$ mA.

motion in the free layer at 0 K is described by the Landau–Lifshitz–Gilbert equation in terms of the spin-transfer torque[8]

$$\frac{d\hat{s}_2}{dt} = \gamma_0 \hat{s}_2 \times \mathbf{H}_{eff} - \alpha \hat{s}_2 \times \frac{d\hat{s}_2}{dt} + \beta_{ST} I \ \hat{s}_2 \times (\hat{s}_1 \times \hat{s}_2) \qquad (2)$$

where $\hat{s}_2$ and $\hat{s}_1$, respectively, denote the unit vectors parallel to the spin direction of the free and pinned layers, γ_0 (<0) is the gyromagnetic ratio, $\mathbf{H}_{eff}$ is the effective magnetic field and α is the damping factor. The first term causes precession of $\hat{s}_2$ around the effective magnetic field. The second term causes a reduction in the precession angle. The third term represents the spin-transfer torque (β_{ST} is the spin-transfer torque coefficient). The sample current (I) comprises the d.c. bias current ($I_{d.c.}$) and a sample RF signal current ($\delta I_{RF} \sin\omega t$). The sample RF current is related to the input RF signal current (δi_{RF}) in the transmission line, and this relation can be expressed as $\delta I_{RF} = \eta \delta i_{RF}$, where η is a factor that corrects current reduction caused by impedance mismatch. By solving equation (2) to the second order of the precession angle, two types of response to the sample RF current are obtained at resonant frequency:

$$\delta\theta_{12}(t) = \delta\theta_{RF} \sin\omega t + \delta\theta_{d.c.}$$

$$\delta\theta_{RF} = -\frac{\sin\theta_{12}}{\Delta\omega} \frac{\partial(\beta_{ST} I)}{\partial I} \delta I_{RF}$$

$$\delta\theta_{d.c.} \cong -\frac{1}{4}(\delta\theta_{RF})^2 \frac{\partial}{\partial\theta} \ln\left(\det[\tilde{\Omega}]\right) \qquad (3)$$

where $\Delta\omega$ is the spectral linewidth, expressed as $\Delta\omega = \Delta\omega_0 + I(2\beta_{ST}\cos\theta_{12} + (\partial\beta_{ST}/\partial\theta_{12})\sin\theta_{12})$, and $\Delta\omega_0$ is the spectral linewidth under zero bias current. $\tilde{\Omega}$ is a tensor that is obtained as a second covariant derivative of the magnetization-potential energy, U (Methods). The resonant frequency, ω_0, is obtained from $\omega_0^2 = \det[\tilde{\Omega}]$ evaluated at the equilibrium point $\delta\theta_{RF}$ is the first-order response to the RF current, which expresses the precession angle of the free-layer spin, whereas $\delta\theta_{d.c.}$ is the second-order response, which expresses the shift in the precession centre. Both responses contribute to the detection of the RF signals as follows[24]

$$V_{detect} = \frac{1}{2}\left(\frac{\partial R}{\partial\theta_{12}}\delta\theta_{RF}\right)\delta I_{RF} + \left(\frac{\partial R}{\partial\theta_{12}}\delta\theta_{d.c.}\right) I_{d.c.} \qquad (4)$$

The first term in equation (4) represents the homodyne detection of the sample RF current because of the resistance oscillation that originates from the sample RF current itself[20]. The second term represents the contribution of the nonlinear FMR, explained as follows: when the FMR in a free-layer spin is excited in an asymmetric potential, the centre of the precession orbital should be energy dependent because of the higher-order nonlinear terms. The basic concept underlying the highly sensitive detection of RF input based on nonlinear FMR is illustrated in Fig. 1a. Without RF input, the free-layer magnetization is at the lowest energy equilibrium point (blue point/arrow in Fig. 1a). Application of a resonant RF signal excites precession motion (orange point/arrow). Owing to the asymmetric potential, the centre position of the high-energy orbital is different from that of the low-energy orbital. This causes a change in the relative angle between the free-layer magnetization and the pinned-layer magnetization and, consequently, a change in the d.c. resistance. Owing to the applied d.c. current bias, the d.c. resistance change results in a large d.c. detection signal. In equation (3), the angle dependence of the resonant frequency, $\partial(\det[\tilde{\Omega}])/\partial\theta$, represents the asymmetry of the potential function.

As mentioned earlier, under zero d.c. bias, the RF detection voltage is explained by the homodyne detection expressed in the

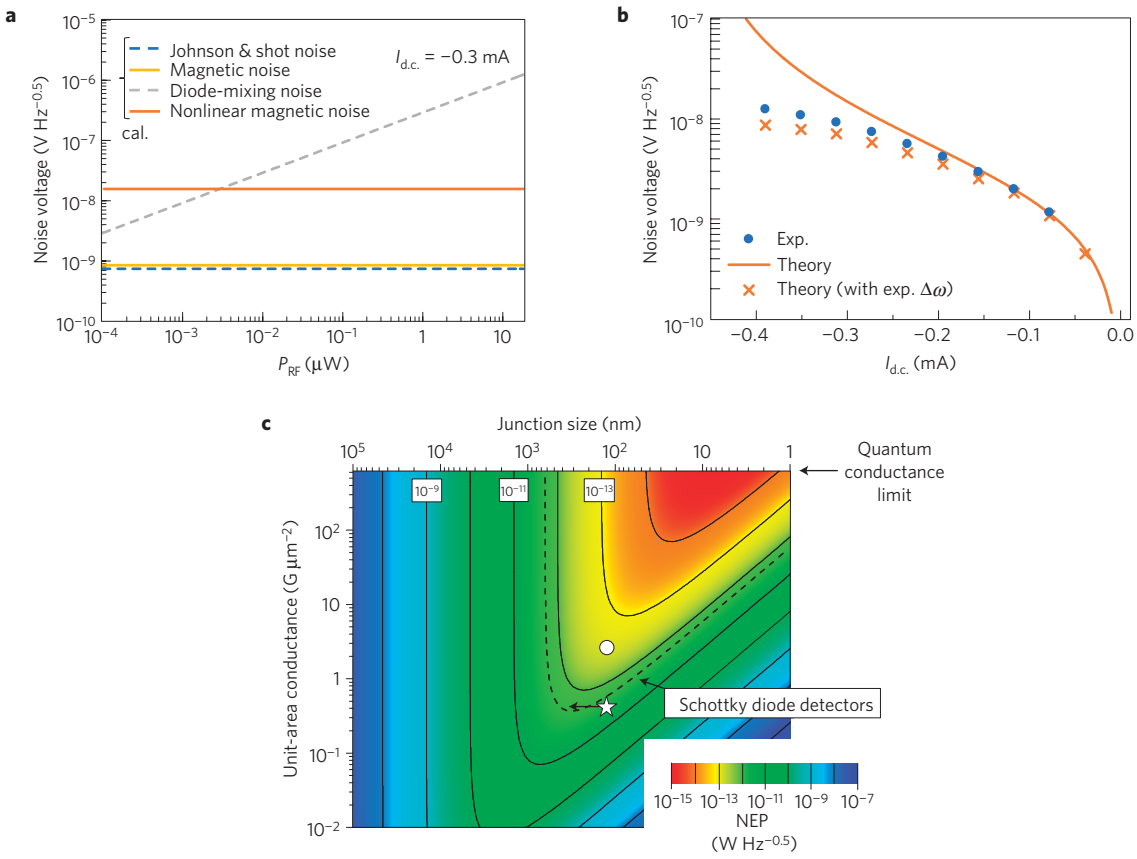

Figure 4 | Noise characteristics. a, Noise voltages around 0 Hz as a function of the RF input power (P_{RF}) estimated by theory. For a small RF input, the dominant contribution is the nonlinear magnetic noise. **b**, d.c. bias ($I_{d.c.}$) dependence of the nonlinear magnetic noise around 0 Hz, which is well reproduced by theory (Supplementary equation (18)). **c**, The NEP. The white star represents the MTJs in this study. It is possible to obtain an NEP as small as the Schottky diode detectors (black dotted curve) by modifying the junction size (black arrow). The white circle represents the value for the MTJ with the highest reported unit-area conductance[40,41]. As the junction size decreases, the nonlinear FMR (Fig. 1a) enhances signals more than noise. Therefore, increasing the unit-area conductance and lowering the junction size is effective for obtaining superior NEP values.

first term of equation (4). On the other hand, the detection by the enhancement of the RF detection voltage under d.c. bias is a kind of power detection, where the average resistance change due to the nonlinear FMR, expressed in the second term of equation (4), is converted to a voltage change by the d.c. bias current. The orange solid curve in Fig. 3a shows the detection voltage calculated from equation (4). For the calculation, all parameters were determined from independent experiments (Methods), and no fitting parameter was employed; nevertheless, the theory was found to reproduce the enhancement, and reasonable agreement was obtained for currents well below the critical current. As the theory neglects the high-order nonlinear terms and thermal fluctuations, the spectral linewidth is zero and the detection voltage is infinite at $I_{d.c.} = I_c$. In the experiment, however, the enhancement was saturated before the d.c. bias reached the critical current. This phenomenon occurred because the reduction of the spectral linewidth was limited, as shown in Fig. 3c. This can be attributed to thermal fluctuations[34], the contribution of high-order nonlinear terms, and the effect of the internal degree of freedom in the magnetic cell. The grey dashed curve in Fig. 3a shows the results of the macro-spin simulation performed for the system at room temperature (Methods). In the simulation, which incorporates thermal fluctuation and high-order nonlinear terms, the divergence behaviour is suppressed and the result obtained by the simulation provides a better explanation for the experimental results than that calculated from equation (4). The macro-spin simulation shows that magnetization auto-oscillations occur under d.c. bias currents larger than the critical current. The inconsistencies between the simulation and experimental results indicate that the macro-spin model is not a good approximation under large d.c. bias. It seems that this can be partially explained by the creation of magnetic domains due to the production of a curly magnetic field by the large current[35].

Another type of nonlinear FMR (called stochastic resonance or thermally assisted FMR), in which the interaction between thermal excitation and spin torque plays a central role, has been observed[29]. In thermally assisted FMR, an applied RF current excites the dynamics between two stable states separated by an energy barrier with the assistance of thermal energy. In the phenomenon, the RF detection voltage may show an exponential dependence on the RF input current. However, for the nonlinear FMR with asymmetric potential discussed in this Article, the device exhibits quadratic detection properties for small RF input ($<10^{-2}$ μW at −0.3 mA as shown in Fig. 3b) and is well described by the theory at 0 K. Hence, the underlying physics in this study is completely different from that of thermally assisted magnetic resonance (see Supplementary Information 2).

Here we discuss other possible mechanisms that may contribute to the rectification output. The stray field from pinned-layer magnetization, field-like torque[20] and voltage-induced magnetic anisotropy change[36] are known to provide a dispersion-shaped spectrum for this configuration. From Fig. 2c, the component of the dispersion shape is less than 10%, therefore, these mechanisms are not dominant in our study. From our estimation,

the influence of the spin motive force[37] is also negligible (see Supplementary Information 2).

Four kinds of noise are found in the RF detectors based on MTJs, namely Johnson and shot noise, magnetic noise[33,38], diode-mixing noise[39] and nonlinear magnetic noise (see Supplementary Information 3). Figure 4a shows the theoretical values of each noise voltage around 0 Hz as a function of the input RF power. When a large RF input power is applied, the MTJs do not show good noise characteristics because the diode-mixing noise is dominant and proportional to the input RF power. On the other hand, the nonlinear magnetic noise governs the noise properties for the low RF input power limit, and better performance in the MTJs than in semiconductors could be expected. The d.c. bias dependence of the nonlinear magnetic noise at ~0 Hz is characterized and shown in Fig. 4b. Under large d.c. bias, theoretical values (Supplementary equation (18)), solid orange curve) are greater than those of the experimental ones (blue circles). However, the theoretical values that account for the experimentally obtained spectral linewidth (orange crosses) reproduce the experiments.

Finally, a noise equivalent power (NEP) is characterized to evaluate the signal-to-noise ratio in the MTJ. The NEP ($\mathrm{W\,Hz^{-0.5}}$) is defined as the noise voltage ($\mathrm{V\,Hz^{-0.5}}$) divided by the sensitivity ($\mathrm{V\,W^{-1}}$). For a small RF input power limit, the NEP in the MTJs is expressed as

$$\frac{\sqrt{8}\pi\alpha N_e}{g^2}\frac{Z_0}{R_Q}\left(\frac{R_0+Z_0}{Z_0}\right)^2 k_B T\sqrt{\Delta\omega} \qquad (5)$$

where $R_Q(=h/e^2)$ is the quantum resistance, Z_0 (50 Ω) is the characteristic impedance of the emission line, g is the spin-transfer efficiency, $N_e(=S/(\hbar/2))$ is the number of electrons in the free layer, k_B is the Boltzmann constant and T is the temperature. The NEP calculated by equation (5) is shown in Fig. 4c. In the calculation, the unit-area conductance and junction size are taken as the variables. The other physical parameters are assumed to be constant, and identical to those of the MTJs employed in this Article. For the value of the spectral linewidth, we use the experimentally obtained value of $\Delta\omega = 0.022$ GHz (from Fig. 3c at $I_{d.c.} = -0.3$ mA). Note that this theoretical analysis reveals that the nonlinear FMR enhances signals more than noise as the size of the magnetic free layer decreases. Therefore, increasing the unit-area conductance value and employing nanoscale magnets is effective for obtaining better NEP values. The white star represents the MTJs in this study. It is possible to obtain an NEP as small as the Schottky diode detectors (black dotted curve) by modifying the junction size to reduce the resistance mismatch between the device and the transmission line (black arrow). The white circle represents the value for the MTJ with the highest reported unit-area conductance[40,41]. The theory predicts that the room-temperature NEP of the MTJ could far exceed that of the semiconductor limits and may reach thermodynamic limits in ~10-nm-scale junctions (see Supplementary Information 3).

In summary, MTJs with a MgO barrier and a FeB free layer were employed to obtain an RF detection sensitivity of 12,000 $\mathrm{mV\,mW^{-1}}$, which is three times that of semiconductor Schottky diodes. The theoretical analysis reveals that the nonlinear effect enhances signals more than noise as the size of the magnets decreases. Therefore, the signal-to-noise ratio may reach thermodynamic limits in ~10-nm-scale junctions. Our study therefore demonstrates a first example of a spintronic device that outperforms semiconductor devices in terms of basic properties.

Methods

Sample preparation. The structure of the MTJs is as follows: Si substrate/buffer layer/PtMn (15 nm)/$Co_{70}Fe_{30}$ (2.5 nm)/Ru (0.85 nm)/$Co_{60}Fe_{20}B_{20}$ (3 nm)/MgO barrier (1 nm)/$Fe_{80}B_{20}$ (2 nm)/MgO cap (1 nm)/Ta (5 nm)/capping layer, which is prepared using the Canon-ANELVA C-7100 UHV sputtering system. The CoFe/Ru/CoFeB layer is a synthetic ferrimagnetic structure, in which the magnetizations of CoFe and CoFeB align in an anti-parallel configuration. The magnetization of the lower CoFe is pinned unidirectionally by an exchange-biasing field from the PtMn anti-ferromagnetic layer. This hybrid structure is commonly used in magnetoresistive devices to harden the magnetization of the pinned layer. Tunnel junctions are fabricated using optical and electron beam lithography combined with an Ar-ion etching technique and a lift-off process. The designed junction is 120 nm in diameter. The MgO cap layer induces a perpendicular anisotropy in the FeB layer[31]. The resistance of the MgO barrier is much greater than that of the MgO cap (see Supplementary Information 2 and Fig. 2a). The resistance area product in the parallel magnetization configuration is 2.5 $\Omega\,\mu m^2$, and the in-plane magnetoresistance ratio, defined as $(R_{AP}-R_P)/R_P$, is 86% (see Supplementary Fig. 2b).

Theoretical calculation. Elements in the tensor, $\tilde{\Omega}$, are defined as $\tilde{\Omega}_{ij} = D_i D_j U$, where $D_i U$ is a covariant derivative of the magnetization potential by an ith coordinate of a canonical coordinate system ($x^1 = \phi, x^2 = S(\cos\theta - 1)$, where ($\theta$, ϕ) is the coordinate in a spherical coordinate system that uses the direction of the pinned-layer spin as a north pole as shown in Supplementary Fig. 5). The $\delta\theta_{d.c.}$ in equation (3) is also described as follows.

$$\delta\theta_{d.c.} \cong -\frac{1}{4}(\delta\theta_{RF})^2\frac{\partial}{\partial\theta}\ln\left(\det[\tilde{\Omega}]\right)$$

$$\cong -\frac{1}{2}(\delta\theta_{RF})^2\left(\frac{1}{\omega_0}\frac{\partial\omega_0}{\partial\theta}+\frac{\cot\theta}{2}\left(1+\sin^2\theta\frac{\partial_\theta^2 U}{\partial_\phi^2 U}\right)\right)$$

The angle (θ) dependence of the resonant frequency (ω_0) expresses the asymmetry of the potential. An additional term appears in the second line because of the use of a curved coordinate system. This term can be expressed using Christoffel symbols.

In the calculations, all of the parameters are determined from independent experiments. The magnetization-potential property, which determines the FMR dynamics in a FeB free layer, is obtained from the fit in Fig. 2b. The saturation magnetization in the FeB (1,375 e.m.u. $\mathrm{cm^{-1}}$) is obtained by the vibrating sample magnetometer measurements. α (0.009) is estimated from the fit of the FMR spectral linewidths under a large magnetic field. η (0.26) is derived from the resistance ($2Z_0/(Z_0+R_0)$). $\beta_{ST} = g\hbar/2eS$ is calculated using $g = P/(1+P^2\cos\theta_{12})$, where the spin polarization (P) is obtained from the tunnel magnetoresistance ratio. $\gamma/2\pi(-29.4\ \mathrm{GHz/T})$ is determined by using the literature value of iron. The relative angle ($\theta_{12} = 108°$) between the magnetizations of the free and pinned layers is estimated to reproduce the experimentally obtained critical current ($I_c = -0.42$ mA from Fig. 3c). The macro-spin simulation is achieved by repeating the computations of equation (2). The effect of thermal energy is related to the addition of a random temperature field[42].

Received 22 April 2013; accepted 14 September 2013; published online 20 October 2013

References

1. Baibich, M. N. *et al.* Giant magnetoresistance of (001)Fe/(001)Cr magnetic superlattices. *Phys. Rev. Lett.* **61,** 2472–2475 (1988).
2. Miyazaki, T. & Tezuka, N. Giant magnetic tunneling effect in $Fe/Al_2O_3/Fe$ junction. *J. Magn. Magn. Mater.* **139,** L231–L234 (1995).
3. Moodera, J. S., Kinder, L. R., Wong, T. M. & Meservey, R. Large magnetoresistance at room temperature in ferromagnetic thin film tunnel junctions. *Phys. Rev. Lett.* **74,** 3273–3276 (1995).
4. Yuasa, S., Fukushima, A., Nagahama, T., Ando, K. & Suzuki, Y. High tunnel magnetoresistance at room temperature in fully epitaxial Fe/MgO/Fe tunnel junctions due to coherent spin-polarized tunneling. *Jpn. J. Appl. Phys.* **43,** L588–L590 (2004).
5. Parkin, S. S. P. *et al.* Giant tunneling magnetoresistance at room temperature with MgO (100) tunnel barriers. *Nature Mater.* **3,** 862–867 (2004).
6. Yuasa, S., Nagahama, T., Fukushima, A, Suzuki, Y. & Ando, K. Giant room-temperature magnetoresistance in single-crystal Fe/MgO/Fe magnetic tunnel junctions. *Nature Mater.* **3,** 868–871 (2004).
7. Djayaprawira, D. D. *et al.* 230% room-temperature magnetoresistance in CoFeB/MgO/CoFeB magnetic tunnel junctions. *Appl. Phys. Lett.* **86,** 092502 (2005).
8. Slonczewski, J. C. Current-driven excitation of magnetic multilayers. *J. Magn. Magn. Mater.* **159,** L1–L7 (1996).
9. Berger, L. Emission of spin waves by a magnetic multilayer traversed by a current. *Phys. Rev. B* **54,** 9353–9358 (1996).
10. Myers, E. B., Ralph, D. C., Katine, J. A., Louie, R. A. & Buhrman, R. A. Current-induced switching of domains in magnetic multilayer devices. *Science* **285,** 867–870 (1999).
11. Huai, Y., Albert, F., Nguyen, P., Pakala, M. & Valet, T. Observation of spin-transfer switching in deep submicron-sized and low resistance magnetic tunnel junctions. *Appl. Phys. Lett.* **84,** 3118–3120 (2004).

12. Kubota, H. *et al.* Evaluation of spin-transfer switching in CoFeB/MgO/CoFeB magnetic tunnel junctions. *Jpn. J. Appl. Phys.* **44,** L1237–L1240 (2005).
13. Diao, Z. *et al.* Spin transfer switching and spin polarization in magnetic tunnel junctions with MgO and AlO_x barriers. *Appl. Phys. Lett.* **87,** 232502 (2005).
14. Tsoi, M. *et al.* Excitation of a magnetic multilayer by an electric current. *Phys. Rev. Lett.* **80,** 4281–4284 (1998).
15. Kiselev, S. *et al.* Microwave oscillations of a nanomagnet driven by a spin-polarized current. *Nature* **425,** 380–382 (2003).
16. Deac, A. *et al.* Bias-driven high-power microwave emission from MgO-based tunnel magnetoresistance devices. *Nature Phys.* **4,** 803–809 (2008).
17. Žutić, I., Fbrian, J. & Sarma, S.D. Spin-polarized transport in inhomogeneous magnetic semiconductors: Theory of magnetic/nonmagnetic p–n junctions. *Phys. Rev. Lett.* **88,** 066603 (2002).
18. Kondo, T., Hayafuji, J. & Munekata, H. Investigation of spin voltaic effect in a p–n heterojunction. *J. Appl. Phys.* **45,** L663–L665 (2006).
19. Rangaraju, N., Peters, J. A. & Wessels, B. W. Magnetoamplification in a bipolar magnetic junction transistor. *Phys. Rev. Lett.* **105,** 117202 (2010).
20. Tulapurkar, A. A. *et al.* Spin-torque diode effect in magnetic tunnel junctions. *Nature* **438,** 339–342 (2005).
21. Sankey, J. C. *et al.* Spin-transfer-driven ferromagnetic resonance of individual nanomagnets. *Phys. Rev. Lett.* **96,** 227601 (2006).
22. Sankey, J. C., Cui, Y-T, Sun, J. Z., Slonczewski, J. C., Buhrman, R. A. & Ralph, D. C. Measurement of the spin-transfer-torque vector in magnetic tunnel junctions. *Nature Phys.* **4,** 67–71 (2008).
23. Kubota, H. *et al.* Quantitative measurement of voltage dependence of spin-transfer torque in MgO-based magnetic tunnel junctions. *Nature Phys.* **4,** 37–41 (2008).
24. Wang, C. *et al.* Bias and angular dependence of spin-torque in magnetic tunnel junctions. *Phys. Rev. B* **79,** 224416 (2009).
25. Wang, C., Cui, Y-T., Katine, J. A., Buhrman, R. A. & Ralph, D. C. Time-resolved measurement of spin-transfer-driven ferromagnetic resonance and spin torque in magnetic tunnel junctions. *Nature Phys.* **7,** 496–501 (2011).
26. Wang, C. *et al.* Sensitivity of spin-torque diodes for frequency-tunable resonant microwave detection. *J. Appl. Phys.* **106,** 053905 (2009).
27. Ishibashi, S. *et al.* Large diode sensitivity of CoFeB/MgO/CoFeB magnetic tunnel junctions. *Appl. Phys. Express* **3,** 073001 (2010).
28. Ishibashi, S. *et al.* High spin-torque diode sensitivity in CoFeB/MgO/CoFeB magnetic tunnel junctions under DC bias currents. *IEEE Trans. Magn.* **47,** 3373–3376 (2011).
29. Cheng, X., Boone, C. T., Zhu, J. & Krivorotov, I. N. Nonadiabatic stochastic resonance of a nanomagnet excited by spin torque. *Phys. Rev. Lett.* **105,** 047202 (2010).
30. Zhu, J. *et al.* Voltage-induced ferromagnetic resonance in magnetic tunnel junctions. *Phys. Rev. Lett.* **108,** 197203 (2012).
31. Kubota, H. *et al.* Enhancement of perpendicular magnetic anisotropy in FeB free layers using a thin MgO cap layer. *J. Appl. Phys.* **111,** 07C723 (2012).
32. Miwa, S. *et al.* Nonlinear thermal effect on sub-gigahertz ferromagnetic resonance in magnetic tunnel junction. *Appl. Phys. Lett.* **103,** 042404.
33. Petit, S. *et al.* Spin-torque influence on the high-frequency magnetization fluctuations in magnetic tunnel junctions. *Phys. Rev. Lett.* **98,** 077203 (2007).
34. Kim, J-V., Mistral, Q., Chappert, C., Tiberkevich, V. S. & Slavin, A. N. Line shape distortion in a nonlinear auto-oscillator near generation threshold: application to spin-torque nano-oscillators. *Phys. Rev. Lett.* **100,** 167201 (2008).
35. Lee, K-J., Deac, A., Redon, O., Nozières, J.-P. & Dieny, B. Excitations of incoherent spin-waves due to spin-transfer torque. *Nature Mater.* **3,** 877–881 (2004).
36. Nozaki, T. *et al.* Electric-field-induced ferromagnetic resonance excitation in an ultrathin ferromagnetic metal layer. *Nature Phys.* **8,** 491 (2012).
37. Zhang, S. & Zhang, S. S-L. Generalization of the Landau-Lifshitz-Gilbert equation for conducting ferromagnets. *Phys. Rev. Lett.* **102,** 086601 (2009).
38. Stutzke, N., Burkett, S. L. & Russek, S. E. Temperature and field dependence of high-frequency magnetic noise in spin valve devices. *Appl. Phys. Lett.* **82,** 91–93 (2003).
39. Prokopenko, O. *et al.* Noise properties of a resonance-type spin-torque microwave detector. *Appl. Phys. Lett.* **99,** 032507 (2011).
40. Maehara, H. *et al.* Tunnel magnetoresistance above 170% and resistance-area product of 1 $\Omega(\mu m)^2$ attained by in situ annealing of ultra-thin MgO tunnel barrier. *Appl. Phys. Exp.* **4,** 033002 (2011).
41. Emura, A. *et al. 12th Joint MMM/Intermag Conf. BU-09* (IEEE Magnetic Society and The American Institute of Physics).
42. Brown, W. F. Thermal fluctuations of a single-domain particle. *Phys. Rev.* **130,** 1677–1686 (1963).

Acknowledgements

We thank A. A. Tulapurkar and S. Yakata for discussions. This research was conducted with the financial support of the Grant-in-Aid for Scientific Research (S), No. 23226001 from the Ministry of Education, Culture, Sports, Science and Technology, Japan (MEXT).

Author contributions

S.M. and S.I. performed the experiments and the analysis; they wrote the paper with T.N., N.M. and Y.S.'s appraisals and inputs. H.T. and S.M. conducted the simulations. S.I., T.S., H.K., K.Y., A.F. and S.Y. prepared the samples. E.T. and K.A. helped with the development of the theory and the measurements, respectively. T.T. and H.I conducted the theoretical analysis about the spin motive force. Y.S. conceived and designed the experiment and developed the theory. All authors contributed to the general discussion.

Additional information

Supplementary information is available in the online version of the paper. Reprints and permissions information is available online at www.nature.com/reprints. Correspondence and requests for materials should be addressed to Y.S.

Competing financial interests

The authors declare no competing financial interests.